Genomic and phenotypic diversification of *Pseudomonas aeruginosa* during sustained exposure to a ciliate predator

Nayma Romo Bechara[1], Nikhil Bardeskar[1], Heather A. Hopkins[2], Kasie Raymann*[1]

1. Department of Plant and Microbial Biology, North Carolina State University, Raleigh, NC
2. Department of Biology, University of North Carolina Greensboro, Greensboro, NC

*Corresponding author: Kasie Raymann, ktrayman@ncsu.edu

Abstract

Opportunistic bacterial pathogens often encounter strong selective pressures outside their hosts, yet the evolutionary consequences of long-term predator exposure remain poorly understood. Here, we used experimental evolution to examine how sustained interaction with a eukaryotic predator shapes genomic adaptation, phenotypic diversification, and virulence-associated traits in *Pseudomonas aeruginosa*. Replicate populations of *P. aeruginosa* were evolved for 60 days in the presence or absence of the ciliate predator *Tetrahymena thermophila*, followed by whole-population metagenomic sequencing, isolate-level genome sequencing, and quantitative phenotypic assays. We observed extensive genetic diversification across all populations, with strong signatures of both positive and purifying selection and pervasive parallel evolution at gene and nucleotide levels. Predator-exposed populations accumulated mutations enriched in regulatory, metabolic, and virulence-associated pathways, revealing predictable genomic targets of selection. However, many parallel mutations were shared between predator-exposed and predator-free populations, indicating that adaptation to the abiotic environment represented a dominant selective force. Genotype–phenotype analyses revealed pleiotropic effects and trade-offs linking motility, growth, and virulence-associated traits. Despite pronounced genomic adaptation and coordinated phenotypic shifts, changes in virulence in an *in vivo* host model were modest and context dependent. Taken together, our results indicate that predator exposure can influence evolutionary trajectories in *P. aeruginosa* and highlight the value of extending such approaches across multiple ecological and host contexts.

Significance

Many bacterial pathogens spend much of their evolutionary history outside hosts, where they face intense ecological pressures such as predation. How these pressures shape pathogen evolution and disease potential remains unclear. Using experimental evolution, genomics, and phenotypic analyses, we show that prolonged exposure to a eukaryotic predator drives predictable genetic and phenotypic changes in the opportunistic pathogen *Pseudomonas aeruginosa*. Predator exposure altered regulatory, metabolic, and virulence-associated pathways, yet much adaptation was shared with predator-free populations, highlighting the dominant role of abiotic environments. Although predator-driven evolution reshaped traits linked to motility and growth, its effects on virulence were modest and context dependent. These findings clarify how environmental interactions influence pathogen evolution and underscore the importance of studying pathogens across diverse ecological settings.

Introduction

Pseudomonas aeruginosa is one of the most widely studied opportunistic bacterial pathogens and serves as a model organism for understanding bacterial virulence, host–pathogen interactions, and social evolution in microbial communities. This free-living, Gram-negative species inhabits a remarkably broad range of environments, including soil, freshwater and marine systems, plant surfaces, animals, and humans (Silby et al. 2011; Wu and Li 2015; Crone et al. 2020; Diggle and Whiteley 2020). Its ecological versatility is largely attributed to a large and flexible genome that encodes diverse metabolic pathways, regulatory networks, and virulence factors, enabling rapid adaptation to distinct niches (Stover et al. 2000; Coggan and Wolfgang 2012; Aroca Molina et al. 2024). Clinically, *P. aeruginosa* is a major concern as a leading cause of opportunistic and nosocomial infections and a significant contributor to morbidity and mortality in patients with cystic fibrosis (Kerr and Snelling 2009).

The evolutionary and ecological success of *P. aeruginosa* is shaped by its capacity to respond rapidly to environmental pressures. Experimental evolution studies have shown

that nutrient limitation, growth in biofilms, chronic infection-like conditions, and interactions with other microbes or phages can drive predictable genetic changes, including loss-of-function mutations in quorum-sensing regulators such as *lasR* (Hammond et al. 2015; Mould et al. 2020) and alterations in genes associated with virulence (Wong et al. 2012; Scribner et al. 2022). Predator-mediated selection, in particular, influences traits closely linked to pathogenicity, including biofilm formation, motility, toxin production, and cooperative behaviors (Matz et al. 2008; Friman et al. 2013; Friman and Buckling 2014). Together, these findings support the hypothesis of coincidental evolution (Levin 1996), which proposes that virulence in opportunistic pathogens often arises outside the host as a by-product of traits selected for environmental survival, including defense against predators such as amoebae, protists, and bacteriophages (Hosseinidoust et al. 2013; Leong et al. 2022; Hopkins et al. 2024).

Despite growing evidence that environmental selection can shape virulence-related traits, few studies have examined how long-term exposure to eukaryotic predators influences both the genomic and phenotypic evolution of *P. aeruginosa*. Coculture experiments with amoebae, *Acanthamoeba castellanii*, have shown that prolonged predator exposure can either enhance or attenuate virulence-associated phenotypes depending on ecological context (Leong et al. 2022), while experimental evolution in the presence of *Caenorhabditis elegans* demonstrated that host interactions modulate both virulence expression and the strength of selection (Granato et al. 2018). Beyond these studies, however, the evolutionary consequences of sustained interaction with eukaryotic predators remain poorly understood.

Here, we address this gap using experimental evolution to investigate how exposure to a eukaryotic predator shapes virulence and virulence-associated traits in *P. aeruginosa*. Populations were evolved for 60 days in the presence or absence of the ciliate *Tetrahymena thermophila*, followed by whole-population and isolate-level sequencing to identify mutations that accumulated during experimental evolution. We detected strong positive and purifying selection, as well as parallel evolution at both the gene and nucleotide levels across independent populations. In addition, we quantified fitness and

virulence-related phenotypes in evolved isolates. Our results demonstrate that predator presence drives predictable genomic changes in key regulatory and virulence-associated genes and leads to coordinated, context-dependent shifts in traits such as motility, biofilm formation, and growth. Despite substantial genomic adaptation, changes in virulence in a host model were modest, highlighting how predator-driven evolution can shape traits relevant to both environmental survival and pathogenic potential.

Results

Six media-evolved (ME) and six predator-evolved (PE) replicate populations of *P. aeruginosa* strain NRB were maintained by daily passaging. For the PE lines, 4% of each bacterial culture was transferred into fresh axenic *T. thermophila* cultures each day to minimize predator–prey co-evolution. Successful transfer of *P. aeruginosa* was confirmed by plating on LB agar. The viability and cell density of the *T. thermophila* cultures were assessed before each passage using light microscopy.

All six PE and six ME populations were subjected to whole-genome shotgun (WGS) metagenomic sequencing on Day 60. In addition, the ancestral strain and individual isolates from each of the 12 evolved populations (ME Lines 1–6 and PE Lines 1–6) were sequenced using WGS sequencing. We then performed phenotypic assays on the evolved isolates (ME = 6 and PE = 6) to attempt to assign mutations to phenotypes.

Mutation patterns in PE and ME populations

Mutations in the evolved populations were identified by comparison to the ancestral genome. The ancestral *P. aeruginosa* strain used in this study was obtained from Carolina Biological Supply; because its precise strain identity was not specified, we sequenced the isolate to both confirm its identity and generate reference genome. Whole-genome comparison revealed that the ancestral strain shares all genes with *P. aeruginosa* FDAARGOS_1041 (GenBank CP065966.1) and is 99.996% identical at the nucleotide level, corresponding to approximately 274 nucleotide differences. To generate a reliable reference, the ancestral strain was sequenced using both long-read (Nanopore) and short-read (Illumina) technologies, and the reads were assembled with hybridSPAdes v3.15.3

(Antipov et al. 2016) to produce a consensus genome. To reduce false-positive variant calls arising from sequencing or assembly errors, all ancestral short reads (average of 215X coverage) were mapped back to the consensus genome using breseq v0.39.0 (Deatherage and Barrick 2014). Any variants detected in the ancestral strain during this mapping were considered potential sequencing or assembly artifacts and were excluded from the subsequent analyses of mutations in the evolved populations.

A total of 972 distinct mutations (frequency >5%) were identified across all evolved lines, excluding same-site parallel mutations. The number of mutations per population ranged from 10 to 169, with average mutation frequencies between 10% and 79% (Figure 1A; Dataset S1). The total number of mutations within a population was not correlated with average mutation frequency (Figure 1A: R^2=0.3209, P=0.0548) or average genome coverage (Figure 1B, Table S1: R^2=0.0006, P=0.9415). Together, these nonsignificant correlations suggest that our sequencing depth was sufficient to capture the mutations present in the populations.

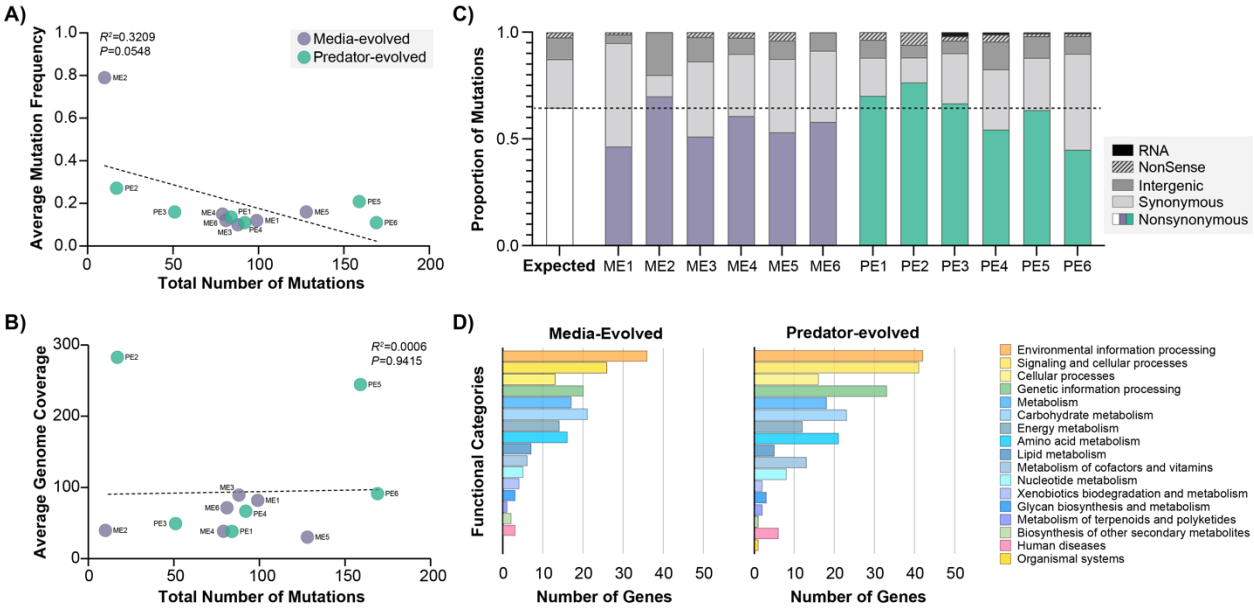

Figure 1. Mutation profiles in evolved populations. A) Relationship between average mutation frequency and the total number of mutations per evolved population. B) Relationship between average genome coverage and the total number of mutations per evolved population. For panels A and B, R^2 values and P-values were calculated using simple linear regression. C) Expected versus observed proportions of mutation types (nonsynonymous, synonymous, intergenic, and other mutation types) in each population. D) Functional annotation of coding-region mutations assigned

to KEGG Orthology (KEGG) functions in media-evolved (ME) and predator-evolved (PE) lines; noncoding and unassigned mutations are not shown. See Dataset S1 for a complete list of identified mutations.

122 In every evolved population, mutations were categorized as nonsynonymous,
123 synonymous, RNA, or intergenic (Figure 1C; Dataset S1). To estimate the expected
124 proportions of nonsynonymous, synonymous, intergenic, nonsense, and RNA mutations
125 under random mutation, we conducted 10,000 independent simulations on the ancestral
126 genome using the Jukes–Cantor model (Jukes and Cantor 1969). The proportion of
127 nonsynonymous mutations in the evolved lines ranged from 44.9% to 76.5%, compared
128 with an expected 64.7% under random mutation (Figure 1C). Five of the six ME lines (all
129 except ME2) and two PE lines (PE4 and PE5) contained fewer nonsynonymous mutations
130 than expected, suggesting purifying selection. By contrast, one ME line (ME2) and two PE
131 lines (PE1 and PE2) showed an excess of nonsynonymous mutations, consistent with
132 positive selection. Two PE lines (PE3 and PE5) had proportions close to the random
133 expectation (Figure 1C).

134 Across the PE lines, 561 total mutations were identified, including those also present in ME
135 lines (i.e., shared mutations), of which 404 occurred in coding regions and 247 could be
136 assigned a KEGG Orthology (KO) annotation (Figure 1D). In the ME lines, 457 mutations
137 were identified, including shared mutations, with 311 in coding regions and 194 assigned
138 KO annotations (Figure 1D). Overall, the PE lines had a higher proportion of mutations in
139 genes associated with Signaling and Cellular Processes, Genetic Information Processing,
140 Metabolism of Cofactors and Vitamins, Nucleotide Metabolism, Human Diseases, and
141 Organismal Systems than the ME lines.

142 We additionally detected strong signatures of positive selection in our populations,
143 reflected by numerous cases of parallel evolution. Parallel evolution events were defined
144 as mutations that arose at the same site or within the same gene in independently evolved
145 lineages (ME, PE, or both). Notably, none of these events were shared across all
146 populations, indicating that the variants were not present in the ancestral genotype. In the
147 ME populations, we identified 34 site-specific parallel mutations occurring in 7 genes,

148 along with 12 gene-level parallel mutations distributed across 6 genes (Figure 2A–B). In the
149 PE populations, we detected 10 site-specific parallel mutations in 4 genes and 35 gene-
150 level parallel mutations in 17 genes (Figure 2A and 2C). Additionally, ME and PE
151 populations shared 113 site-specific parallel mutations spanning 10 genes and 287 gene-
152 level parallel mutations across 40 genes (Figure 2A), 178 of which occurred in the same
153 gene *blp2* (Dataset S1). Most parallel mutations were present at relatively low frequencies
154 (<20%); however, several reached high frequencies (>60%) or were fixed, including
155 mutations in *mgtE*, *phoQ*, and *clpA* in ME lines and in *siaB*, *wbpM*, and *fha1* in PE lines
156 (Figure 2B–C, Dataset S1). Parallel mutations are extremely unlikely to occur by chance
157 and constitute strong evidence of positive selection. In addition, the vast majority of the
158 high frequency (>60%) parallel mutations affected nonsynonymous positions (92%), which
159 further suggests that these mutations are adaptive.

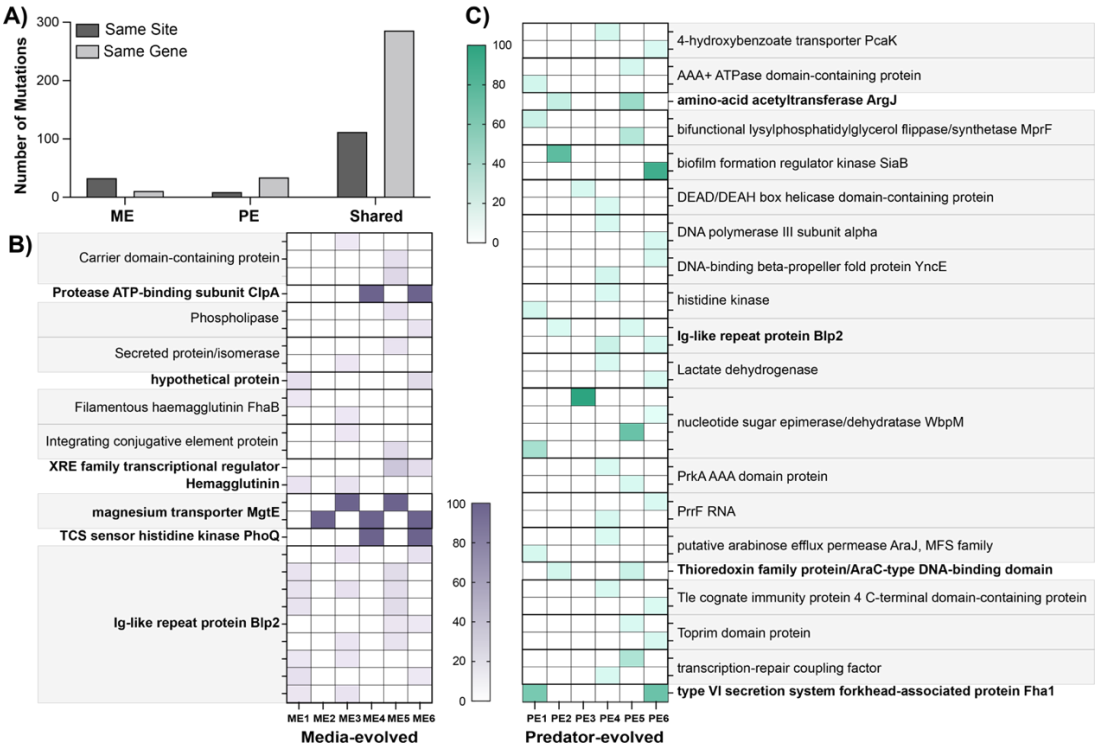

Figure 2. Parallel evolution events in evolved populations. A) Number of fixed, same-site and same-gene parallel mutations in predator-evolved (PE) and media-evolved (ME) populations, as well as mutations shared between both groups. B–C) Frequency of site-specific and gene-specific parallel mutations in (B) ME and (C) PE populations; genes in which site-specific parallel mutations occurred are indicated in bold font and gene-specific parallel mutations are highlighted in gray. For a list of all mutations identified in the evolved populations see Dataset S1.

160

Genomic and phenotypic characterization of evolved isolates

A single isolate was collected from each population (n = 12). Analysis of each isolate revealed between three and seven mutations per genome, and each isolate carried at least one mutation that was also fixed in its corresponding population (Figure 2A–B and Figure 3A). In total, 46 mutations were identified across 24 genes, and several instances of parallel evolution were detected (Figure 3A, Dataset S2).

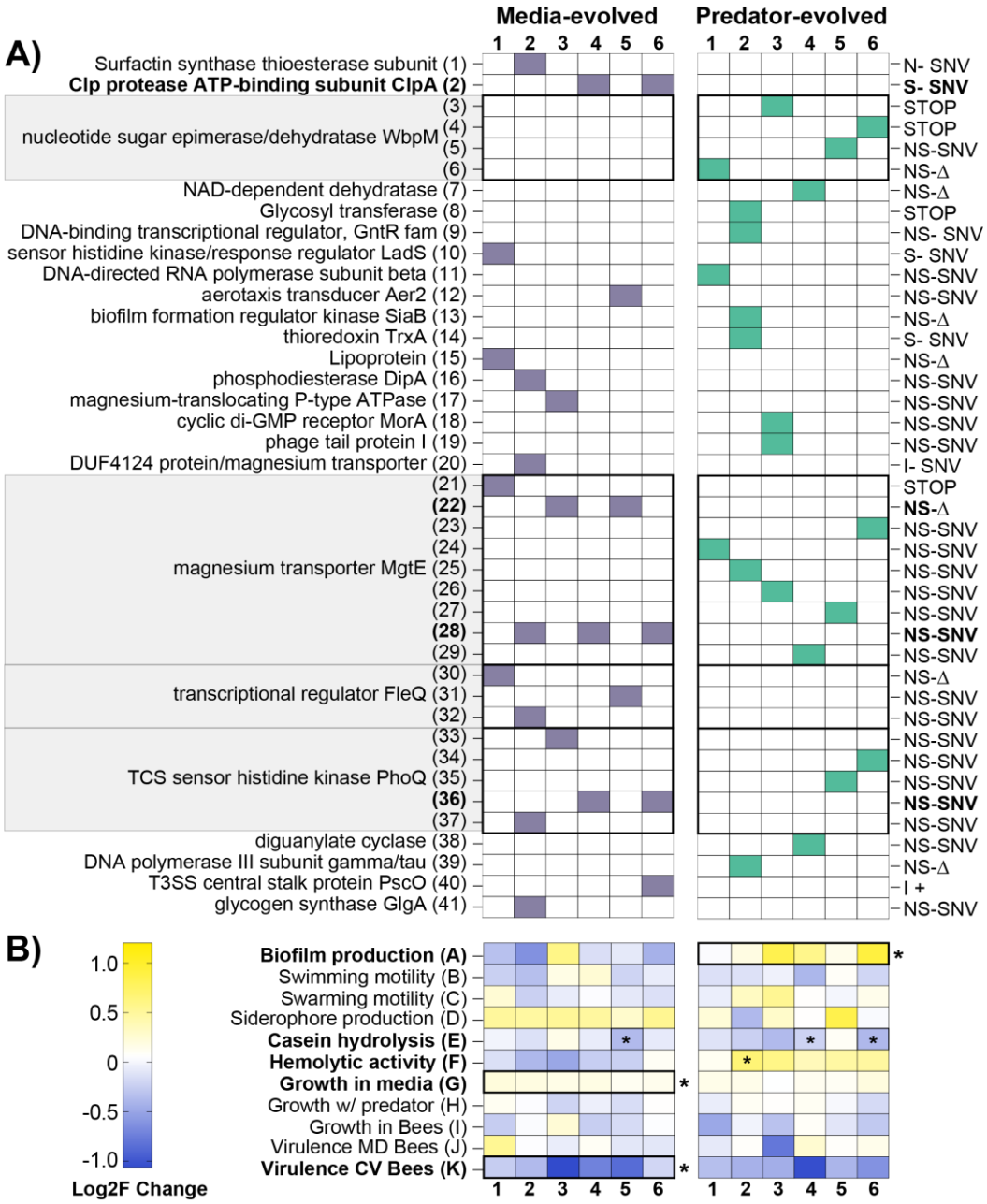

Figure 3. Genotypic and phenotypic changes in evolved isolates. A) Mutations identified in evolved isolates, highlighting site-specific parallel mutations (bold font) and gene-specific parallel mutations (outlined boxes) unique to predator-evolved (PE) and media-evolved (ME) isolates. NS, nonsynonymous; S, synonymous; I, intergenic; STOP, nonsense; SNV, single-nucleotide variant; Δ, deletion; +, insertion. For a list of all mutations identified in the evolved isolates see Dataset S2. B) Log_2 fold change calculated from the mean of all replicates and trials for each phenotype measured in evolved isolates relative to the ancestral strain. Yellow indicates an increase, blue indicates a decrease, and white indicates no change. Asterisks within boxes indicate significant differences when individual isolates were compared to the ancestor, whereas asterisks in the margin indicate significant differences when the mean of all ME lines or all PE lines was compared to the ancestral mean. Bold text denotes phenotypes showing significant changes relative to the ancestor. Statistical significance was determined using a Kruskal–Wallis test with Dunn's multiple-comparison test ($P < 0.05$). Full data for all replicates, including non-log_2 fold-change values, are shown in Figures S1 and S2**.**

167 Among the ME isolates, site-specific parallel mutations occurred in *clpA* and *phoQ*, both
168 present in ME4 and ME6. A site-specific parallel mutation in *mgtE* was also found in ME2,
169 ME4, and ME6. In addition, a gene-specific mutation in *fleQ*, unique to the ME lines,
170 occurred in ME1, ME2, and ME5 (Figure 3A, Dataset S2). In the PE isolates, a gene-specific
171 mutation in *wbpM*, unique to the PE lines, was identified in PE1, PE2, PE5, and PE6. Finally,
172 two gene-specific mutations, *mgtE* and *phoQ*, were shared between ME and PE isolates
173 (Figure 3A, Dataset S2).

174 To assess the impact of predator-driven evolution on *P. aeruginosa*, we performed
175 phenotypic assays on a single isolate from each evolved population, allowing direct
176 correlation with mutations identified via genomic analysis. Virulence-associated traits,
177 including biofilm production, motility, siderophore production, casein hydrolysis, and
178 hemolytic activity, were measured (Figure 3B, Figure S1 A–F). Fitness was evaluated in two
179 different conditions: growth after 24 h in media and in coculture with *T. thermophila* (Figure
180 3B, Figure S1G–H). All assays were performed in at least triplicate.

181 After correcting for multiple comparisons, only a few isolates differed significantly from the
182 ancestor for any of the phenotypes tested. Specifically, isolates ME5, PE4, and PE6
183 exhibited reduced casein hydrolysis, indicating decreased extracellular protease activity
184 involved in protein degradation (Figure 3B), whereas isolate PE2 showed significantly
185 increased hemolytic activity compared to the ancestral strain (Figure 3B). When comparing

186 the mean of all PE or ME isolates to the ancestor, PE isolates showed higher biofilm
187 production and ME isolates exhibited increased growth in media (Figure 3B; Figure S1G).

188 Although not statistically significant, additional patterns were observed. Swimming activity
189 (Figure 3B) decreased in most D60-evolved lines, with the exception of ME3 and ME4.
190 Swarming activity (Figure 3B) was generally reduced in ME isolates, except ME1, but
191 increased in most PE isolates relative to the ancestor. For biochemical traits, most evolved
192 isolates produced slightly more siderophore (Figure 3B), with PE2 as the exception.
193 Protease activity decreased on average in both ME and PE lines, except for a slight increase
194 in D60-ME6. Hemolytic activity decreased in all ME lines, whereas PE lines exhibited an
195 increase (Figure 3B).

196 To evaluate how predation impacted *P. aeruginosa* virulence, we used a tractable
197 invertebrate host model, the honey bee (*Apis mellifera*) (Figure 3B, Figure S2). We
198 performed two types of assays: one in conventional (CV) honey bees, which were healthy
199 adults with an intact microbiome (Figure S2A), and another in microbiota-depleted (MD)
200 bees (Figure S2B). The MD bees were newly emerged (~1 day old) adults of the same age.

201 All PE and ME isolates displayed a decrease in virulence in CV bees, although this was not
202 significant after multiple comparisons. In MD bees, most ME isolates showed a slight
203 decrease in virulence compared to the ancestor, with the exception of ME1. Among the PE
204 isolates, four (PE2, PE4, PE5, and PE6) showed a slight increase, PE1 showed no change,
205 and PE3 showed a slight decrease. Overall, in CV bees, the average virulence of all PE
206 isolates did not differ from the ancestor, whereas the average virulence of all ME isolates
207 was significantly reduced (Figure S2A). In MD bees, no significant differences in virulence
208 were observed for either group compared to the ancestor (Figure S2B).

209 To determine whether the attenuated virulence was due to reduced proliferation in the
210 honey bee gut, we performed growth assays for each isolate in MD bees (Figure 3B, Figure
211 S2). While the mean growth levels showed trends that loosely resembled the virulence
212 patterns observed in MD bees (Figure S2A), no statistically significant differences in growth
213 were detected for either ME or PE isolates. Instead, both groups exhibited substantial

214 isolate-to-isolate variation. In each group, three of the six replicates showed a slight
215 increase in growth (ME2, ME3, ME6; PE2, PE4, PE5), whereas the remaining three showed a
216 slight decrease (ME1, ME4, ME5; PE1, PE3, PE6) relative to the ancestor.

217 We next analyzed genotype–phenotype correlations and found that a subset of mutations
218 was strongly associated with changes in multiple functional traits (Figure 4A, Dataset S3).
219 For example, mutation 28 in *mgtE* was negatively correlated with biofilm production while
220 mutation 22, also in *mgtE*, was negatively correlated with virulence in CV bees. Mutations
221 3, 18, 19, and 26 (located in *wbpM*, *morA*, a phage tail protein, and *mgtE*) displayed
222 identical patterns across phenotypes, showing significant positive correlations with
223 swarming and significant negative correlations with growth in media and virulence in MD
224 honey bees.

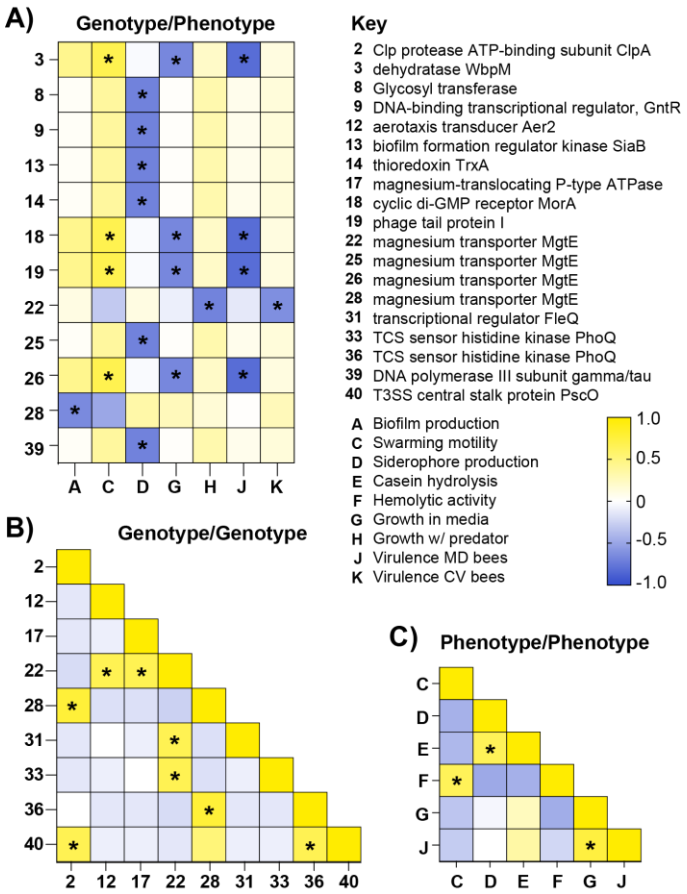

Figure 4. Correlations between genotypes and phenotypes in evolved isolates. A) Correlations between individual mutations and phenotypic traits. B) Correlations among identified mutations. C) Correlations among phenotypic traits. Yellow represents a positive correlation, blue represents

a negative correlation, white means no correlation, and asterisks (*) indicate statistical significance, $P < 0.05$. Statistical significance was assessed using Spearman's rank correlation. See Dataset S3 for complete list of Spearman r and P-values.

Genotype–genotype correlations (Figure 4B, Dataset S3) revealed that several mutations were positively associated, suggesting preferred evolutionary trajectories. The phenotype–phenotype correlation matrix (Figure 4C, Dataset S3) showed that certain traits were significantly positively coupled, including swarming motility and hemolytic activity, siderophore production and casein hydrolysis, and growth in media and virulence in MD bees.

In addition to individual fitness assays, we performed competition experiments by coculturing all isolates for 20 h in media, in the presence of *T. thermophila*, and in honey bees (Figure 5). Whole-genome metagenomic sequencing was then used to determine which strains outcompeted the others in each condition. In the presence of the predator, ME3 and ME4 outperformed all other lines. In media, ME2, ME3, ME4, and ME6 outcompeted the other isolates and the ancestor. In honey bee competitions, ME4 prevailed over all other isolates and the ancestral strain (Figure 5).

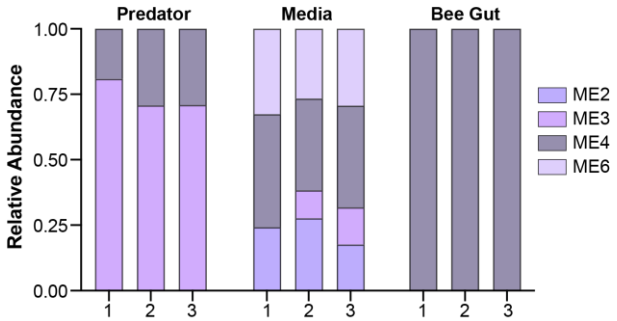

Figure 5. Competition assays with the evolved isolates and the ancestral strain in the presence of a predator, in media, or in honey bee host. Each assay was performed in triplicate.

Discussion

The emergence of virulence and other adaptations in opportunistic bacterial pathogens, particularly *P. aeruginosa*, has been widely studied under diverse selective conditions, including copper exposure (12 days), antibiotic treatment (30 days), oxidative stress (12 days), and in presence of amoeboid and nematode predators (*A. castellanii*, 42 days and

243 nematode *C. elegans*, 60 days) (Granato et al. 2018; Laborda et al. 2022; Lear et al. 2022;
244 Leong et al. 2022; Fu et al. 2023). While predator pressure is predicted to indirectly select
245 for increased virulence, the two studies that have evaluated this in *P. aeruginosa* generally
246 found reduced virulence (Granato et al. 2018; Leong et al. 2022). However, the impact of a
247 ciliate predator on *P. aeruginosa* evolution has not been systematically explored. Here, we
248 investigated the influence of the generalist ciliate predator *T. thermophila* on the virulence,
249 fitness, and genomic evolution of *P. aeruginosa* over a 60-day experimental evolution
250 period. By combining WGS metagenomics of evolved populations and isolates with *in vitro*
251 and *in vivo* phenotypic assays, we provide insight into how predation shapes bacterial
252 evolution at both the genotypic and phenotypic levels.

253 Our WGS analyses revealed extensive genetic diversification across the ME and PE
254 populations. A total of 457 mutations were identified in ME lines and 561 in PE lines, with
255 numerous cases of parallel evolution at both the site and gene level. The observation of
256 parallel mutations at high frequency in genes such as *mgtE*, *phoQ*, and *clpA* in ME lines
257 and in *siaB*, *wbpM*, and *fha1* in PE lines indicates strong selective pressures acting on
258 specific functional pathways. Interestingly, while several lines showed evidence of
259 purifying selection, other lines exhibited an excess of nonsynonymous mutations,
260 consistent with positive selection. These patterns highlight that adaptation can proceed
261 via both constraint and innovation and that even replicate populations evolving under the
262 same conditions can follow distinct evolutionary trajectories.

263 KEGG pathway analysis indicated that PE populations were enriched for mutations in
264 genes associated with signaling, metabolism, and genetic information processing. This
265 enrichment suggests that exposure to predation selects for modifications in critical
266 regulatory and metabolic functions that may enhance survival under predatory pressure.
267 However, adaptation to the media appears to be the dominant selective force, as reflected
268 by the large number of parallel mutations shared between ME and PE lines and the
269 substantial number of mutations unique to ME lines. This may indicate that this strain of *P.*
270 *aeruginosa* already possesses effective mechanisms to defend against or avoid predation,

271 reducing the relative impact of predator-driven selection compared with nutrient-based
272 adaptation.

273 Analysis of individual isolates (*n* = 12) revealed 46 mutations across 24 genes, with
274 evidence of selective sweeps at identical positions or within the same genes across lines.
275 Notably, mutations in *mgtE*, *phoQ*, *fleQ*, and *wbpM* were recurrent across multiple lines,
276 suggesting that these genes are key targets of selection. *FleQ*, a master regulator of
277 flagellar motility and biofilm formation, was mutated in ME1, ME2, and ME5, coinciding
278 with reductions in both swimming motility and biofilm production. This is consistent with
279 previous studies showing that *FleQ* modulates motility and exopolysaccharide
280 biosynthesis in a context-dependent manner (Arora et al. 1997; Hickman and Harwood
281 2008). Mutations in *phoQ*, part of the PhoP–PhoQ two-component regulatory system
282 (Gellatly et al. 2012), were found in several ME and PE lines and likely contributed to
283 attenuated virulence, particularly in conventional honey bees. Conversely, mutations in
284 *mgtE*, a dual-function magnesium transporter linked to type III secretion system regulation
285 (Anderson et al. 2010; Coffey et al. 2014), were present in all isolates. While *mgtE*
286 mutations can enhance virulence, in our study most lines exhibited reduced virulence,
287 except for ME1, PE4, and PE6, suggesting that the phenotypic outcome depends on the
288 precise mutation location and genetic context. In ME1, a stop codon in *mgtE*, combined
289 with a mutation in *ladS*, a kinase regulating the acute-to-chronic virulence (Broder et al.
290 2016), likely contributed to its elevated virulence. Mutations in *wbpM* were observed in
291 most PE isolates but none of the ME isolates, highlighting a potential role in adaptation to
292 predation. *WbpM* is involved in O-antigen synthesis (Burrows et al. 2000), and while only
293 PE6 displayed increased virulence relative to the ancestor, other mutations in *wbpM* may
294 confer advantages against predation, potentially via enhanced biofilm formation or altered
295 surface interactions.

296 Our genotype–phenotype correlation analysis indicates that phenotypic diversification in
297 this system is driven by a limited number of mutations with broad, pleiotropic effects
298 rather than by many mutations each affecting a single trait. In particular, distinct mutations
299 within mgtE were associated with different functional outcomes, with one mutation

300 negatively correlated with biofilm formation and another specifically linked to reduced
301 virulence in CV bees, highlighting functional heterogeneity within this locus. In contrast,
302 mutations in wbpM, morA, a phage tail protein, and mgtE exhibited highly concordant
303 phenotypic signatures, characterized by increased swarming motility coupled with
304 reduced growth in rich media and decreased virulence in MD honey bees. This repeated
305 association of motility gains with fitness trade-offs suggests that these mutations may shift
306 resource allocation toward dispersal at the expense of host-associated performance. The
307 presence of strong positive genotype–genotype correlations further implies that these
308 mutations do not arise independently but instead form preferred evolutionary
309 combinations, potentially reflecting shared selective pressures or epistatic compatibility.
310 Finally, the observed coupling among phenotypic traits, such as swarming with hemolytic
311 activity and growth in media with virulence, supports the idea that ecological and
312 pathogenic traits are evolutionarily linked, constraining the range of accessible adaptive
313 strategies. Collectively, these patterns suggest that pleiotropic mutations and correlated
314 trait responses interact to bias evolutionary trajectories toward a restricted subset of
315 genetic and phenotypic outcomes.

316 Using CV and MD honey bees as in vivo models, we observed context-dependent virulence
317 outcomes. While all evolved isolates showed decreased virulence in CV bees, ME isolates
318 were significantly attenuated on average. In MD bees, phenotypic variation was greater,
319 with some PE isolates showing slight increases in virulence. Growth assays in MD bees
320 revealed only nonsignificant trends in gut proliferation, with no consistent or significant
321 differences among isolates, indicating that reduced virulence cannot be attributed to an
322 individual isolate's ability to proliferate in the honey bee gut. Instead, these results suggest
323 that changes in specific virulence factors, rather than overall bacterial fitness, drive host
324 outcomes. It is important to note that *P. aeruginosa* is not a natural pathogen of honey
325 bees, and the virulence effects observed in this host may not fully reflect outcomes in
326 mammalian systems. Indeed, our evolved lines could exhibit differential virulence in
327 mammalian hosts, as some phenotypic changes, such as increased hemolytic activity,
328 would have minimal impact on bees, which lack red blood cells, but could enhance

329 pathogenicity in vertebrate hosts. However, testing these potential effects in mammals
330 was beyond the scope of the current study.

331 Competition assays demonstrated that predator-driven evolution shaped competitive
332 outcomes in environment-specific ways by decreasing its fitness, as ME isolates
333 dominated all three competition environments. These findings suggest that adaptation to
334 predation impair fitness under selective pressure but may incur trade-offs under
335 alternative conditions, consistent with ecological theory on specialization versus
336 generalist strategies.

337 Overall, our results illustrate that long-term exposure to a eukaryotic predator can drive
338 predictable patterns of parallel evolution in *P. aeruginosa*, with distinct genotypic and
339 phenotypic consequences. However, the large number of parallel mutations shared
340 between ME and PE lines suggests that adaptation to the media exerted a stronger
341 selective force than predator-specific pressures. Comparing these findings to our previous
342 60-day experimental evolution study of *Serratia marcescens* under *T. thermophila*
343 predation (Hopkins et al. 2024) highlights both shared and divergent patterns. In *S.*
344 *marcescens*, predator-evolved lines maintained or enhanced virulence and grazing
345 resistance, exhibited increased biofilm production, and accumulated many more
346 mutations specific to predator-evolved lines, indicating stronger adaptation to predation
347 than in *P. aeruginosa*. By contrast, *P. aeruginosa* PE populations showed more variable
348 phenotypic responses, with virulence generally decreasing but biofilm production
349 increasing. These differences in virulence may also reflect host specificity, as *S.*
350 *marcescens* is a natural pathogen of honey bees, whereas *P. aeruginosa* is not known to
351 naturally infect this host. Together, these results suggest that the relative impact of
352 predator-specific versus general environmental selection can differ between opportunistic
353 bacteria, reflecting species-specific differences in ecological strategy, phenotypic
354 plasticity, and the balance between nutrient adaptation and predation.

355 Although our 60-day evolution period revealed substantial genetic and phenotypic
356 changes, longer-term experiments may uncover additional adaptive mutations that require

357 more generations to become fixed. Future studies could explore how these evolutionary
358 dynamics manifest in complex microbial communities, across different host species, or
359 under fluctuating environmental conditions. The functional analyses of key genes, such as
360 *mgtE*, *phoQ*, and *wbpM*, will also help elucidate the molecular mechanisms linking
361 predator-driven evolution to virulence and ecological fitness.

362 **Methods**

363 *Experimental evolution*

364 The ancestral *P. aeruginosa* strain we used for our experiments was purchased from
365 Carolina Biological Supply Company and evolved either in media alone (ME) or in the
366 presence of the protist predator *T. thermophila* strain SB210 (PE). *T. thermophila* was
367 obtained from the Tetrahymena Stock Center at Cornell University. Each evolution
368 treatment included six replicate lines.

369 Prior to starting the evolution experiment, *T. thermophila* and ancestral *P. aeruginosa* were
370 cultured individually for 72 h and 48 h, respectively, at 35°C in Neff media. To initiate each
371 evolved line, 1 OD of *P. aeruginosa* was resuspended in fresh Neff media, and 0.12 mL was
372 added to either 3 mL of Neff media alone (ME lines) or 3 mL of Neff media containing *T.*
373 *thermophila* (PE lines). The starting ratio of bacteria to predator was determined in
374 preliminary trials to allow both organisms to persist in co-culture for 24 h.

375 Experimental cultures (3 mL) were incubated at 35°C with shaking. Every 24 h for 180 days,
376 cultures were vortexed and 4% of each line was transferred into fresh Neff media (ME lines)
377 or new axenic *T. thermophila* cultures (PE lines). Prior to each transfer, *T. thermophila*
378 viability and density were assessed using light microscopy, and *P. aeruginosa* growth was
379 confirmed by plating on LB agar. Throughout the experiment, both organisms were
380 consistently present, and no noticeable changes in population size were observed based
381 on daily growth and plating. On day 60, agar plates were inoculated from each culture, and
382 one colony was randomly selected from each ME (ME1–6) and PE population (PE1–6). Each
383 colony was grown in 3 mL LB broth for 48 h at 35°C to obtain pure cultures. A 200 µL aliquot
384 of each culture was frozen at –80°C in 20% glycerol. These 12 isolates were subsequently

385 sequenced and used for phenotypic assays, including virulence in bees, growth assays,
386 biochemical tests, biofilm production, and competition experiments.

387 *DNA extraction and sequencing*

388 Cultures of the evolved populations (ME1–6 and PE1–6), evolved isolates (ME1–6 and PE1–
389 6), and the ancestral strain were diluted to 1 OD, and DNA was extracted using the Zymo
390 Quick-DNA™ Miniprep Plus Kit (D4069). Libraries for short-read sequencing were prepared
391 using the Illumina Nextera DNA Flex Library Prep Kit (20018704). The ancestral genome
392 was sequenced using both long-read (Oxford Nanopore MinION) and short-read (Illumina
393 iSeq100) technologies. Evolved populations and isolates were sequenced using short-read
394 Illumina platforms (iSeq100 or MiSeq100) with 2 × 150 bp paired-end reads.

395 *Genome assembly and analysis*

396 The Illumina and Nanopore reads of the ancestral genome were combined to generate a
397 hybrid assembly using hybridSPAdes v3.15.3 (Antipov et al. 2016). Assembled scaffolds
398 were annotated with Bakta (Schwengers et al. 2021) on the Department of Energy Systems
399 Biology Knowledgebase (KBase) platform. Genome sequence comparisons were
400 performed between the ancestral strain and the three closest related strains, identified
401 based on BLAST searches against the NCBI database. Average nucleotide identity values
402 were calculated using FastANI v1.32 (Jain et al. 2018). A pangenome analysis was
403 conducted using Panaroo v1.5.2 (Tonkin-Hill et al. 2020) with the following parameters: an
404 initial clustering threshold of 0.98 using CD-HIT, a family threshold of 0.7 for secondary
405 clustering of orthologous genes into gene families, a length difference percentage cutoff of
406 0.80, a core gene threshold of 1 (genes present in all genomes), strict clean mode, and
407 removal of invalid genes. All short reads of the ancestral strain were then mapped back to
408 the consensus genome using breseq v0.39.0 (Deatherage and Barrick 2014). Any variants
409 identified during this mapping were considered sequencing or assembly artifacts and were
410 excluded from the set of candidate mutations in the evolved populations and isolates.

411 Sequencing reads from the evolved populations and isolates were trimmed using
412 Trimmomatic v0.40 (Bolger et al. 2014) and subsequently mapped to the assembled

413 ancestral genome using breseq v0.39.0 (Deatherage and Barrick 2014), with a base-quality
414 cutoff of PHRED 30 and a minimum frequency cutoff of 0.05 to identify mutations. Once
415 identified, mutations were compared against the ancestral strain using gdtools
416 (Deatherage and Barrick 2014).

417 To assess the expected distribution of mutations under neutrality, we performed 10,000
418 independent simulations using a custom Python script. Each simulation introduced a
419 single mutation at random under a Jukes–Cantor model in our *P. aeruginosa* reference
420 genome. Genome annotations were used to classify mutations as intergenic or coding. The
421 coding mutations were further classified as synonymous or nonsynonymous by comparing
422 the translated protein sequence before and after the mutation. The functional
423 characterization of genes was predicted using KOALA KEGG Orthology and Links
424 Annotation (Kanehisa 2000; Kanehisa et al. 2016).

425 *Phenotypic assays*

426 **Growth in media:** Cultures of evolved populations (ME1–6 and PE1–6), evolved isolates
427 (ME1–6 and PE1–6), and the ancestral strain were diluted to 1 OD. For each isolate, 0.12
428 mL of culture was added to 3 mL fresh Neff media in triplicate and incubated at 35°C with
429 shaking at 110 rpm. After 24 h, cultures were diluted and plated on cetrimide agar in
430 duplicate. Plates were incubated for 48 h at 35°C, and colonies were counted to calculate
431 CFUs.

432 **Growth in the presence of *T. thermophila*:** Axenic 48-h cultures of *T. thermophila* in Neff
433 media were inoculated with 120 µL of 1 OD cultures of each isolate in triplicate. Cultures
434 were incubated for 20 h at 35°C and 110 rpm, diluted, and plated on cetrimide agar in
435 duplicate. Plates were incubated for 48 h at 35°C before counting colonies and calculating
436 CFUs.

437 **Growth in-host:** Pupae were collected 2–3 days before emergence and kept in cages with
438 sterile sugar syrup (SSS) and sterile pollen. Newly emerged adult bees were hand-fed 10 µL
439 of either sterile SSS, the ancestor in SSS, or an evolved isolate in SSS (5 bees per cup, 15
440 bees per treatment). Bees were maintained at 35°C and 95% humidity. After 20 h, guts

441 were collected, stored in 20% glycerol at –80°C, and dilutions up to 10^{-6} were performed
442 and plated on cetrimide agar in triplicate. Plates were incubated 48 h at 35°C, colonies
443 were counted, and CFUs/mL were calculated based on the dilution factor.

444 **Biofilm assay:** Biofilm formation was assessed in triplicate. First, 5 µL of 1 OD cultures
445 were added to 150 µL Neff media in 96-well microplates with an additional sterile
446 nonskirted plate immersed into the wells to provide a bigger surface attachment; this
447 setup was incubated at 35°C for 24 h without shaking. Wells and the immersed plate were
448 washed twice with sterile ddH_2O, stained with 150 µL of 0.1% crystal violet for 15 min,
449 washed again, and air-dried. Biofilms in both microplates (initial and immersed) were
450 separately solubilized with 150 µL of 30% acetic acid, and absorbance was measured at
451 490 nm. The measurements were combined to obtain a final reading. Three independent
452 assays were performed, each with four replicates.

453 **Casein hydrolysis:** Milk agar plates were prepared by mixing 2.5 g yeast extract and 7.5 g
454 agar in 350 mL water and 15 g milk powder in 150 mL water; both solutions were
455 autoclaved, cooled, mixed, and poured into plates. Sterile discs were inoculated with 4 µL
456 of 1 OD bacterial culture and incubated at 37°C for 48 h. To assess protease activity, the
457 plates were photographed and analyzed using ImageJ by calculating the diameter of the
458 activity and subtracting the 4-mm diameter of the disc.

459 **Siderophore production:** CAS-CTAB agar plates were prepared by dissolving 0.065 g
460 Chromeazurol S (CAS) in 50 mL water and 0.0729 g CTAB in 40 mL water. Those two
461 solutions were then mixed with 10 mL of 1 mM $FeCl_3$ hexahydrate and 10 mM HCl solution
462 and added to LB agar medium, followed by pH adjustment to 6.8 and autoclaving. Sterile
463 discs were placed and inoculated with 4 µL of 1 OD bacterial culture and incubated at
464 37°C for 48 h. For analyzing siderophore production, plate photographs were uploaded to
465 ImageJ to measure the diameter of the siderophore production minus the diameter of the
466 disc (4 mm).

467 **Hemolytic activity:** Blood agar plates (LB + 5% sheep blood) were inoculated with 4 µL of 1
468 OD bacteria and incubated at 37°C for 48 h before assessing hemolysis, as previously
469 described in the siderophore production protocol.

470 **Swimming and swarming motility:** Swim plates contained peptone (5 g), yeast extract (3
471 g), and 0.3% agar per liter of water; swarm plates used 0.5% agar. Plates were autoclaved,
472 poured, and allowed to solidify for up to 24 h. The plates were stab-inoculated with 2 µL of
473 1 OD culture and incubated at 37°C for 48 h before measuring motility by measuring the
474 diameter of the motion in photographs uploaded to ImageJ.

475 *Virulence assay in honey bees*

476 **Conventional bees:** Pure 1 OD cultures of each evolved isolate and the ancestor were
477 centrifuged (10,000 rpm × 2 min) and individually resuspended 1:1 in SSS. Adult worker
478 bees (*A. mellifera*) were collected from a single hive at the Phytotron, NCSU, Raleigh, NC,
479 and immobilized at 4°C. Bees were randomly distributed into groups and exposed via the
480 immersion method (~10 µL per bee) to one of three treatments: 1) sterile SSS only, 2) the
481 ancestor in SSS, or 3) each evolved isolate in SSS. Bees were maintained in cup cages (20
482 bees/cup; 100 bees/treatment) under hive-like conditions (35°C, 95% humidity). Mortality
483 was recorded daily for 5 days. Two independent assays were performed, each with five
484 replicates, totaling 200 bees per isolate.

485 **Microbiota-depleted bees:** Each evolved isolate was first cultured to 1 OD_{600}, followed by
486 centrifugation to pellet the bacteria and resuspension of the pellet in 1:1 SSS. Newly
487 emerged honey bees (*A. millifera*) were immobilized at 4°C and randomly distributed in
488 different 50-mL Falcon tubes. Ten bees were added to a single tube, in which isolate-
489 containing SSS was added (10 µL per bee) for immersion treatment. Every isolate,
490 ancestor, and control treatment was performed in triplicate (i.e., 10 bees × 3 = 30 bees per
491 treatment). The treated bees were then maintained in cup cages under hive-like conditions
492 (35°C and 95% humidity) for 5 days, and mortality was recorded. Two independent assays
493 were performed, totaling 60 bees per isolate.

494 *Competition assays*

495 **In-host competition:** Pupae were collected 2–3 days prior to emergence from a single hive
496 at the Phytotron (NCSU) and maintained in cages with SSS and sterile pollen. After
497 emergence, cultures of each evolved isolate and the ancestor were normalized to OD_{600} =
498 1, centrifuged (10,000 rpm for 2 min), and resuspended in SSS. For inoculation, strains
499 were pooled such that the ancestor and each evolved isolate (ME1–6 and PE1–6) were
500 present in equal proportions. A total of 25 bees were hand-fed 10 µL of the bacterial
501 suspension in SSS and maintained in cup cages (5 bees per cup; 5 cups total) at 35°C and
502 95% humidity. After 20 h, bee guts were collected under sterile conditions and stored in
503 20% glycerol at –80°C. Although all bees were sampled, three individual bee gut samples
504 (each from a different cup cage) were selected for downstream analysis. These samples
505 were plated on cetrimide agar in triplicate, incubated for 24 h, and ~300 colonies per
506 sample were pooled in 1× PBS. DNA was extracted from the pooled colonies and analyzed
507 by WGS metagenomic sequencing (2x150 PE reads on Illumina miSeq100). Reads were
508 mapped to the ancestral genome using breseq v0.39.0 (Deatherage and Barrick 2014), and
509 gdtools (part of the breseq pipeline) was used to compare each sample to mutations
510 present in the ancestor and the individual evolved isolates (ME1–6 and PE1–6). The relative
511 frequency of each strain was estimated as the average frequency of mutations shared
512 between the isolate and the sample.

513 **Competition in the presence of *T. thermophila*:** Five replicate tubes containing 3 mL of *T.*
514 *thermophila* in Neff media were inoculated with 0.12 mL of 1 OD mixture of all evolved
515 isolates and the ancestor. Cultures were incubated for 20 h at 35°C with shaking at 110
516 rpm. Three replicate samples were diluted and plated in triplicate on cetrimide agar,
517 incubated for 48 h at 35°C, and ~300 colonies per sample were collected in 1 mL of 1×
518 PBS. DNA was extracted from the pooled colonies, sequenced, and analyzed following the
519 protocol stated above for **in-host competition**.

520 **Competition in media:** Five replicate tubes containing 3 mL of Neff media were inoculated
521 with 0.12 mL of 1 OD mixture of the ancestor and evolved isolates. After 20 h of incubation
522 at 35°C and 110 rpm, three of the replicate cultures were centrifuged at 10,000 rpm for 2
523 min. Supernatants were discarded, and pellets were resuspended in 200 µL of 1× PBS.

524 DNA was extracted from the pooled colonies (~300 colonies per sample), sequenced, and
525 analyzed following the protocol described above for **in-host competition**.

526 *Statistical analyses*

527 All figures and statistical analyses were performed in GraphPad Prism v10.5.0. Figures
528 were visually improved using Adobe Illustrator.

529 **Mutations:** The relationship between the total number of mutations per evolved
530 population and (i) average genome coverage and (ii) average number of mutations was
531 assessed using simple linear regression (see Figure 1A–B).

532 **Phenotypic analyses:** For all phenotypic assays, significance between each evolved line
533 and the ancestral strain was assessed using a Kruskal–Wallis test, followed by Dunn's
534 multiple-comparison test, incorporating both technical and biological replicates (see
535 Figure 3B, Figure S1 and Figure S2). In addition, the mean phenotypic values of all ME lines
536 combined and all PE lines combined were each compared to the ancestral mean using a
537 Kruskal–Wallis test with Dunn's multiple-comparison test to assess differences between
538 evolved groups relative to the ancestor (see Figure 3B, Figure S1, and Figure S2).

539 **Genotype and phenotype correlations**: **Genotype–phenotype correlations:** All
540 mutations detected in evolved isolates were scored as binary variables (1 = present, 0 =
541 absent) for each evolved line. For phenotypic traits, means were calculated across all
542 biological and technical replicates, and $\log_2$ fold changes relative to the ancestral
543 phenotype were determined. Binary mutation presence/absence data and phenotypic $\log_2$
544 fold-change values were then used to identify significant correlations across evolved lines
545 between (i) mutations and phenotypes (genotype–phenotype), (ii) mutations and other
546 mutations (genotype–genotype), and (iii) phenotypes and other phenotypes (phenotype–
547 phenotype) using Spearman's rank correlation coefficient (ρ). All Spearman's ρ values and
548 corresponding P-values are provided in Dataset S2.

549 **Data availability**

The complete genome of the ancestral strain has been deposited in NCBI under BioProject PRJNA1387885. All raw sequencing data for evolved populations and isolates have been deposited in the NCBI Sequence Read Archive (SRA) under BioProject PRJNA1390225. All other data are included in the main text and supplementary material. Bacterial strains and evolved populations are available from the authors upon reasonable request.

Acknowledgements

We thank Marcos Garcia for his assistance with the experiments. We are grateful to Dr. Awa Diop for assistance in classifying the ancestral strain used in this study. We also thank Dr. Louis-Marie Bobay, Dr. Parul Bardeskar, and Patrick Gallagher for their careful reading of the manuscript and helpful editorial suggestions. This work was supported by the National Institutes of Health under grant 7R01GM145747 (to K.R.).

561 ## References

562 Anderson GG, Yahr TL, Lovewell RR, O'Toole GA. 2010. The Pseudomonas aeruginosa
563 magnesium transporter MgtE inhibits transcription of the type III secretion system.
564 *Infect. Immun.* 78:1239–1249.

565 Antipov D, Korobeynikov A, McLean JS, Pevzner PA. 2016. HYBRID SPADES: an algorithm for
566 hybrid assembly of short and long reads. *Bioinformatics* 32:1009–1015.

567 Aroca Molina KJ, Gutiérrez SJ, Benítez-Campo N, Correa A. 2024. Genomic differences
568 associated with resistance and virulence in Pseudomonas aeruginosa isolates from
569 clinical and environmental sites. *Microorganisms* 12:1116.

570 Arora SK, Ritchings BW, Almira EC, Lory S, Ramphal R. 1997. A transcriptional activator,
571 FleQ, regulates mucin adhesion and flagellar gene expression in Pseudomonas
572 aeruginosa in a cascade manner. *J. Bacteriol.* 179:5574–5581.

573 Bolger AM, Lohse M, Usadel B. 2014. Trimmomatic: a flexible trimmer for Illumina
574 sequence data. *Bioinformatics* 30:2114–2120.

575 Broder UN, Jaeger T, Jenal U. 2016. LadS is a calcium-responsive kinase that induces
576 acute-to-chronic virulence switch in Pseudomonas aeruginosa. *Nat. Microbiol.*
577 2:16184.

578 Burrows LL, Urbanic RV, Lam JS. 2000. Functional conservation of the polysaccharide
579 biosynthetic protein WbpM and its homologues in Pseudomonas aeruginosa and
580 other medically significant bacteria. *Infect. Immun.* 68:931–936.

581 Coffey BM, Akhand SS, Anderson GG. 2014. MgtE is a dual-function protein in
582 Pseudomonas aeruginosa. *Microbiology* 160:1200–1213.

583 Coggan KA, Wolfgang MC. 2012. Global regulatory pathways and cross-talk control
584 Pseudomonas aeruginosa environmental lifestyle and Virulence phenotype. *Curr.*
585 *Issues Mol. Biol.* 14:47–70.

586 Crone S, Vives-Flórez M, Kvich L, Saunders AM, Malone M, Nicolaisen MH, Martínez-García
587 E, Rojas-Acosta C, Catalina Gomez-Puerto M, Calum H, et al. 2020. The
588 environmental occurrence of Pseudomonas aeruginosa. *APMIS* 128:220–231.

589 Deatherage DE, Barrick JE. 2014. Identification of mutations in laboratory-evolved
590 microbes from next-generation sequencing data using breseq. *Methods Mol. Biol.*
591 *Clifton NJ* 1151:165–188.

592 Diggle SP, Whiteley M. 2020. Microbe profile: Pseudomonas aeruginosa: opportunistic
593 pathogen and lab rat. *Microbiology* 166:30–33.

594 Friman V-P, Buckling A. 2014. Phages can constrain protist predation-driven attenuation of
595 Pseudomonas aeruginosa virulence in multienemy communities. *ISME J.* 8:1820–
596 1830.

597 Friman V-P, Diggle SP, Buckling A. 2013. Protist predation can favour cooperation within
598 bacterial species. *Biol. Lett.* 9:20130548.

599 Fu T, Gifford DR, Knight CG, Brockhurst MA. 2023. Eco-evolutionary dynamics of
600 experimental Pseudomonas aeruginosa populations under oxidative stress.
601 *Microbiol. Read. Engl.* 169:001396.

602 Gellatly SL, Needham B, Madera L, Trent MS, Hancock REW. 2012. The Pseudomonas
603 aeruginosa PhoP-PhoQ two-component regulatory system is induced upon
604 interaction with epithelial cells and controls cytotoxicity and inflammation. *Infect.*
605 *Immun.* 80:3122–3131.

606 Granato ET, Ziegenhain C, Marvig RL, Kümmerli R. 2018. Low spatial structure and
607 selection against secreted virulence factors attenuates pathogenicity in
608 Pseudomonas aeruginosa. *ISME J.* 12:2907–2918.

609 Hammond JH, Dolben EF, Smith TJ, Bhuju S, Hogan DA. 2015. Links between Anr and
610 quorum sensing in Pseudomonas aeruginosa biofilms. *J Bacteriol.* 197:2810–2820.

611 Hickman JW, Harwood CS. 2008. Identification of FleQ from Pseudomonas aeruginosa as a
612 c-di-GMP-responsive transcription factor. *Mol. Microbiol.* 69:376–389.

613 Hopkins HA, Lopezguerra C, Lau M-J, Raymann K. 2024. Making a pathogen? Evaluating the
614 impact of protist predation on the evolution of virulence in Serratia marcescens.
615 *Genome Biol. Evol.* 16:evae149.

616 Hosseinidoust Z, Tufenkji N, van de Ven TGM. 2013. Predation in homogeneous and
617 heterogeneous phage environments affects virulence determinants of
618 Pseudomonas aeruginosa. *Appl. Environ. Microbiol.* 79:2862–2871.

619 Jain C, Rodriguez-R LM, Phillippy AM, Konstantinidis KT, Aluru S. 2018. High throughput ANI
620 analysis of 90K prokaryotic genomes reveals clear species boundaries. *Nat.*
621 *Commun.* 9:5114.

622 Jukes TH, Cantor CR. 1969. Evolution of protein molecules. In: Munro HN, editor.
623 Mammalian protein metabolism. New York: Academic Press. p. 21–132.

624 Kanehisa M. 2000. KEGG: Kyoto encyclopedia of genes and genomes. *Nucleic Acids Res.*
625 28:27–30.

626 Kanehisa M, Sato Y, Kawashima M, Furumichi M, Tanabe M. 2016. KEGG as a reference
627 resource for gene and protein annotation. *Nucleic Acids Res.* 44:D457–D462.

628 Kerr KG, Snelling AM. 2009. Pseudomonas aeruginosa: a formidable and ever-present
629 adversary. *J. Hosp. Infect.* 73:338–344.

630 Laborda P, Martínez JL, Hernando-Amado S. 2022. Evolution of habitat-dependent
631 antibiotic resistance in Pseudomonas aeruginosa. *Microbiol. Spectr.* 10:e0024722.

632 Lear L, Hesse E, Buckling A, Vos M. 2022. Copper selects for siderophore-mediated
633 virulence in Pseudomonas aeruginosa. *BMC Microbiol.* 22:303.

634 Leong W, Poh WH, Williams J, Lutz C, Hoque MM, Poh YH, Yee BYK, Chua C, Givskov M,
635 Sanderson-Smith M, et al. 2022. Adaptation to an amoeba host leads to
636 Pseudomonas aeruginosa isolates with attenuated virulence. *Appl. Environ.*
637 *Microbiol.* 88:e02322-21.

638 Levin BR. 1996. The evolution and maintenance of virulence in microparasites. *Emerg.*
639 *Infect. Dis.* 2:93–102.

640 Matz C, Moreno AM, Alhede M, Manefield M, Hauser AR, Givskov M, Kjelleberg S. 2008.
641 Pseudomonas aeruginosa uses type III secretion system to kill biofilm-associated
642 amoebae. *ISME J.* 2:843–852.

643 Mould DL, Botelho NJ, Hogan DA. 2020. Intraspecies signaling between common variants
644 of Pseudomonas aeruginosa increases production of quorum-sensing-controlled
645 virulence factors. mBio 11:e01865–20.

646 Schwengers O, Jelonek L, Dieckmann MA, Beyvers S, Blom J, Goesmann A. 2021. Bakta:
647 rapid and standardized annotation of bacterial genomes via alignment-free
648 sequence identification. *Microb. Genomics* 2021:000685

649 Scribner MR, Stephens AC, Huong JL, Richardson AR, Cooper VS. 2022. The nutritional
650 environment is sufficient to select coexisting biofilm and quorum-sensing mutants
651 of Pseudomonas aeruginosa. *J. Bacteriol.* 204:e00444–21.

652 Silby MW, Winstanley C, Godfrey SAC, Levy SB, Jackson RW. 2011. Pseudomonas
653 genomes: diverse and adaptable. *FEMS Microbiol. Rev.* 35:652–680.

654 Stover CK, Pham XQ, Erwin AL, Mizoguchi SD, Warrener P, Hickey MJ, Brinkman FSL,
655 Hufnagle WO, Kowalik DJ, Lagrou M, et al. 2000. Complete genome sequence of
656 Pseudomonas aeruginosa PAO1, an opportunistic pathogen. *Nature* 406:959–964.

657 Tonkin-Hill G, MacAlasdair N, Ruis C, Weimann A, Horesh G, Lees JA, Gladstone RA, Lo S,
658 Beaudoin C, Floto RA, et al. 2020. Producing polished prokaryotic pangenomes with
659 the Panaroo pipeline. *Genome Biol.* 21:180.

660 Wong A, Rodrigue N, Kassen R. 2012. Genomics of adaptation during experimental
661 evolution of the opportunistic pathogen Pseudomonas aeruginosa. *PLoS Genet*.
662 8:e1002928.

663 Wu M, Li X. 2015. Klebsiella pneumoniae and Pseudomonas aeruginosa. In: Tang Y-W,
664 Sussman M, Liu D, Poxton I, Schwartzman J, editors. Molecular medical
665 microbiology (second edition). Boston: Academic Press. p. 1547–1564.
666

667 **Supplemental Material**

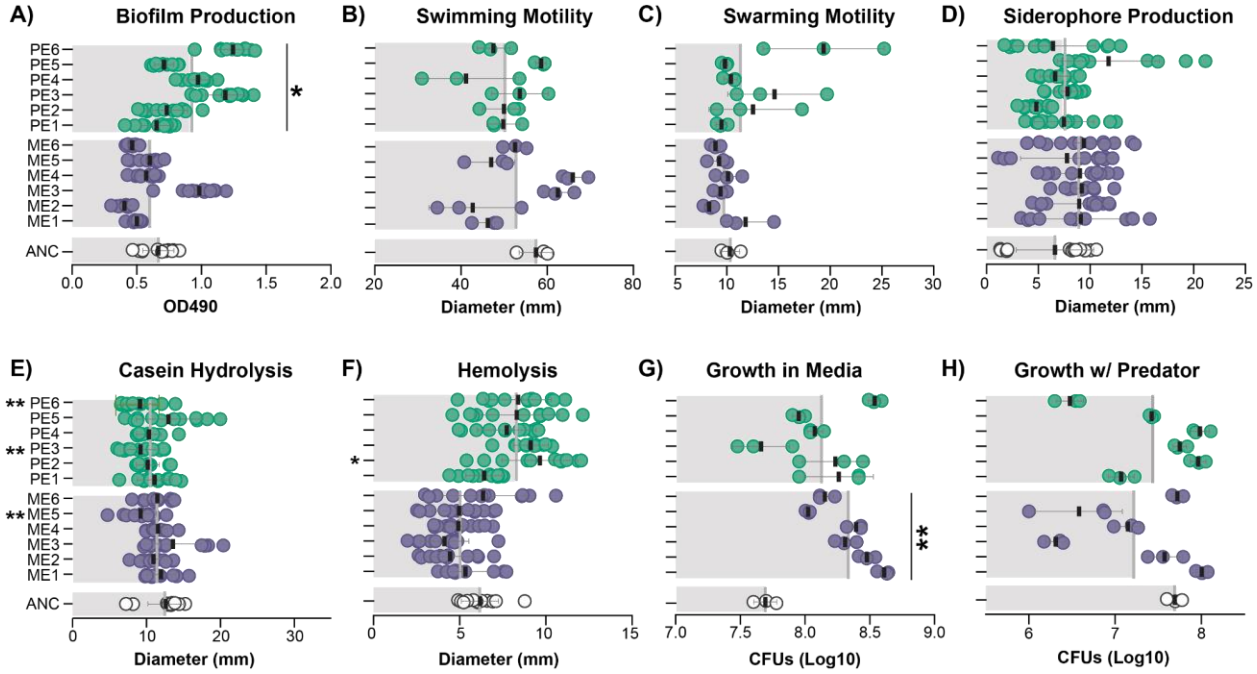

668

669 **Figure S1. Phenotypic characteristics of evolved isolates.** Assays performed were: (A) biofilm
670 production, (B) swimming motility, (C) swarming motility, (D) siderophore production, (E) casein
671 hydrolysis, (F) hemolytic activity, (G) growth in media after 24 h based on CFU counts, and (H)
672 growth in co-culture with *T. thermophila* after 24 h based on CFU counts. Statistical significance
673 was determined using a Kruskal–Wallis test, followed by Dunn's multiple comparisons test. For all
674 analyses, the mean rank of each group was compared to that of the ancestral strain. Comparisons
675 were performed for each evolved isolate individually (asterisks on the left) and for the mean of all
676 ME and PE isolates (asterisks on the right) relative to the mean of the ancestor. *, P < 0.05; **, P <
677 0.01.

678

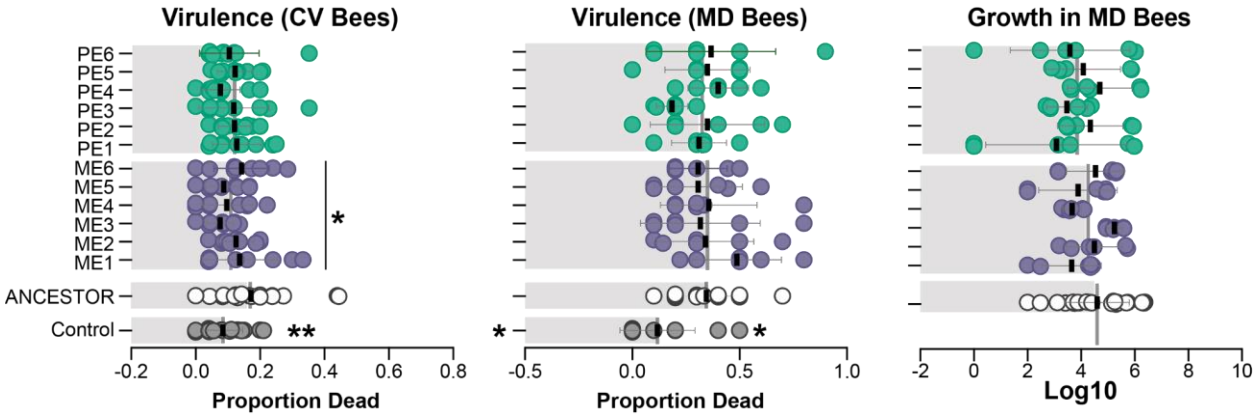

679

680 **Figure S2. Virulence and growth of evolved isolates in honey bees.** Proportion of dead (A)
681 conventional (CV) honey bees and (B) microbiota-depleted (MD) honey bees after 5 days of

682 exposure to the ancestral strain or individual PE and ME isolates. (C) Growth of the ancestor, PE,
683 and ME isolates in microbiota-depleted honey bees based on colony-forming unit (CFU) counts;
684 CFU values are shown as $\log_{10}$-transformed counts. In panels A and B, each data point represents a
685 cup cage containing 20 bees for CV trials and 10 bees for MD trials (biological replicates with
686 technical replication). In panel C, each data point represents an individual bee. Statistical
687 significance was tested both between each individual PE and ME isolate and the ancestral strain,
688 and between the mean of PE and ME isolates and the ancestral strain. Statistical significance was
689 determined using a Kruskal–Wallis test followed by Dunn's multiple comparisons test (*, $P < 0.05$;
690 **, $P < 0.01$).

Sample	Line	Average Coverage	% Aligned
Isolate	PE-1	31.90703	99.45%
Isolate	PE-2	44.70393	99.37%
Isolate	PE-3	32.88026	99.42%
Isolate	PE-4	28.97971	98.98%
Isolate	PE-5	39.65268	98.99%
Isolate	PE-6	24.55709	98.96%
Isolate	ME-1	19.68769	99.06%
Isolate	ME-2	47.9632	99.19%
Isolate	ME-3	93.0591	99.15%
Isolate	ME-4	35.00678	99.02%
Isolate	ME-5	29.0038	98.59%
Isolate	ME-6	55.80903	99.05%
Population	PE-1	38.33171	99.15%
Population	PE-2	282.7614	99.21%
Population	PE-3	49.2864	98.80%
Population	PE-4	66.66734	98.29%
Population	PE-5	244.5668	98.99%
Population	PE-6	91.32875	97.91%
Population	ME-1	81.95025	98.53%
Population	ME-2	39.79088	98.71%
Population	ME-3	89.21901	98.66%
Population	ME-4	38.41933	98.57%
Population	ME-5	30.37836	97.94%
Population	ME-6	71.459	98.28%

691 **Table S1. Average genome coverage of evolved populations and isolates.**

692 **Dataset S1. Mutations identified in evolved populations.** List of mutations detected across all
693 evolved populations at a frequency greater than 5%.

694 **Dataset S2. Mutations identified in evolved isolates.** List of mutations detected across all
695 evolved isolates at a frequency greater than 5%.

Dataset S3. Spearman correlation results for genotype–phenotype, genotype–genotype, and phenotype–phenotype comparisons. Complete Spearman's rank correlation coefficients (ρ) and corresponding P-values for all pairwise comparisons across evolved lines. Mutations were encoded as binary variables (1, present; 0, absent) for each line. Phenotypic values represent means across all biological and technical replicates and are expressed as $\log_2$ fold changes relative to the ancestral phenotype.